Autophosphorylation Dependent Destabilization of the Insulin Receptor Kinase Domain: Tryptophan-1175 Reports Changes in the Catalytic Cleft†

Steven M. Bishop,‡ J. B. Alexander Ross, and Ronald A. Kohanski*

Department of Biochemistry, Box 1020, The Mount Sinai School of Medicine, One Gustave L. Levy Place, New York, New York 10029

Received October 27, 1998; Revised Manuscript Received December 30, 1998

ABSTRACT: Protein kinases are regulated by conformational or chemical changes which facilitate access of substrates to the active site and promote correct orientations of catalytically essential residues and water molecules. The switch between basal and activated states of the insulin receptor's kinase domain (IRKD) results from autophosphorylation. We investigated the effects of IRKD autophosphorylation on the conformational stability by guanidine hydrochloride (GdnHCl) dependent denaturation and by iodide quenching of intrinsic fluorescence. Tryptophan residues of the recombinant soluble IRKD (residues R^{953}−S^{1355}) were excited at a λ_{ex} of 295 nm, and emission spectra were analyzed for centroid (a characteristic of average polarity of the indole rings' environments) and integrated fluorescence intensity over the λ_{em} range of 310−420 nm. Denaturation profiles of both apo- and phospho-IRKD forms are complex with at least three distinct unfolding transitions. The first and last transitions were reversible and cooperative and had midpoints at 0.4 or 0.7 M GdnHCl and 2.4 or 2.7 M GdnHCl, respectively; transitions of phospho-IRKD occurred at lower GdnHCl concentrations. Calculations of free energy of unfolding suggested a loss of ∼2.3 kcal/mol of stabilization for the first transition and ∼1.5 kcal/mol for the third transition. Circular dichroism showed subtle changes in secondary structure over the first transition and global unfolding over the last transition. The first transition reports changes primarily in the local environment of W^{1175}, which is near the catalytic loop and is conserved among protein tyrosine kinases. W^{1175} is also the dominant fluorophore of the native emission spectrum. Iodide quenching of W^{1175} was virtually undetectable in the apo-IRKD but significant in the phospho-IRKD, suggesting that W^{1175} exposure to small solutes is strongly dependent on the conformation of the activation loop. These studies indicate that autophosphorylation, while exposing the catalytic center, also produces a conformer less stable than the apoenzyme.

The insulin receptor is a disulfide-linked heterotetrameric $\alpha_2\beta_2$ transmembrane glycoprotein (*1*). The binding of insulin to the extracellular α-subunits causes autophosphorylation of the intracellular kinase domain of the β-subunits (*2*). This results in activation of signaling through increased kinase activity and substrate recruitment (*3*). The insulin receptor kinase domain [IRKD;[1] R^{953}−S^{1355}, as described by Villalba et al. (*4*) but numbered according to Ebina et al. (*5*)] can be phosphorylated at up to seven sites within three distinct domains (*6*−*10*): Y^{965} and Y^{972} in the juxtamembrane domain, Y^{1158}, Y^{1162}, and Y^{1163} in the activation loop (AL, residues D^{1150}−P^{1172}), and Y^{1328} and Y^{1334} in the carboxy-terminal region. The AL tyrosines are the principle sites responsible for regulating the catalytic efficiency of the IRKD (*11*−*14*).

The crystal structures of the apo and phosphorylated core of the IRKD have been determined (*15*, *16*). The catalytically active core region encompasses V^{978}−K^{1283} and includes the three AL tyrosines. These structures show the spatial organization of the ATP and peptide binding sites, the conserved catalytic loop, and the variable activation loop, which are arranged in or near the cleft within the bilobate scaffold common to all protein kinases. The AL in the apo form appears to act as an autoinhibitory "gate" blocking nucleotide and peptide entry to the active site cleft. This "gate closed" conformation accounts for the high $K_{M,ATP}$ and $K_{M,peptide}$ values reported recently for the basal state apo-IRKD (*17*). The tris-phosphorylated form, cocrystalized with a peptide substrate and ATP analogue, shows the AL swung away from the active site. This "gate open" conformation of the kinase may be the maximally activated state. The gate-open position of the tris-phosphorylated AL seems to be stabilized by intraloop electrostatic interactions between phosphotyrosines (pY^{1162} and pY^{1163}) and neighboring arginyl groups of the AL (R^{1164} and R^{1155}, respectively). The lack of new, strong bonds involving phosphotyrosines of the AL to either of the lobes should suggest that the gate-open

† Supported by Grants DK50074 (R.A.K.) and in part by Grant GM39750 (J.B.A.R.) from the National Institutes of Health.

* To whom correspondence should be addressed. Phone: (212) 241-7288. Fax: (212) 996-7214. E-mail: r_kohanski@smtplink.mssm.edu.

‡ Present address: Department of Pharmaceutical Research and Development, Genentech, Inc., South San Fransisco, CA 94080.

[1] Abbreviations: CD, circular dichroism; CES, centroid of the emission spectrum; DTT, dithiothreitol; EDTA, ethylenediaminetetraacetic acid; FI, fluorescence intensity; GdnHCl, guanidine hydrochloride; IRKD, insulin receptor kinase domain; PAGE, polyacrylamide gel electrophoresis; PCR, polymerase chain reaction. Standard one- and three-letter abbreviations for amino acids are used.

10.1021/bi982546s CCC: $18.00
Published on Web 02/17/1999

conformation of the AL is unlikely to restrict domain movements after autophosphorylation.

Local structural perturbations and global conformational changes can be reported by the spectral characteristics of tryptophan residues (*18*). In addition, the relative solvent accessibility of fluorescent tryptophan residues can be learned by solute quenching (*19*−*21*). Thus, intrinsic fluorescence and quenching are powerful tools for analyzing structural properties of enzymes in different functional states. However, in multi-tryptophan proteins such as the protein kinases, the potential complexity of information available from the emission spectra is greatly increased (reviewed in refs *22* and *23*). The IRKD has five tryptophans; W^{989} is on the surface of the small lobe, and W^{1175}, W^{1193}, W^{1200}, and W^{1246} are in the interior of the large lobe. The fluorescence properties of these tryptophan residues change during GdnHCl dependent denaturation in ways that reveal the differences in global and local structural stabilities of the basal state apo-IRKD versus the activated state phospho-IRKD. Trp-to-Phe replacement mutagenesis allowed us to identify the active site tryptophan as the principle fluorescence emitter. Furthermore, iodide quenching provides evidence of local conformational changes related to the gate opening associated with autophosphorylation. Together, these studies provide new insight into the conformational states and stabilities of protein tyrosine kinases and the environment of the catalytic cleft.

EXPERIMENTAL PROCEDURES

Materials. ATP (disodium salt from equine muscle) and DTT (SigmaUltra) were from Sigma. Hydrogenated Triton-X100 (protein grade) was from Calbiochem. EDTA was from Fluka. Tris acetate, base, and HCl were from Boeringer Mannheim. GdnHCl (extreme purity grade) was from Heico Chemicals, Inc. Magnesium acetate (enzyme grade), potassium iodide (ACS grade), potassium chloride (ACS grade), sodium thiosulfate (ACS grade), and reagents for subcloning were from Fisher. Restriction endonucleases were from New England Biolabs.

Recombinant Cytoplasmic Kinase Domain Cloning, Expression, and Purification. Construction of the subcloning vectors p72CKD and pXCKD, encoding insulin receptor residues Arg^{953}−Ser^{1355}, were described previously (*24*). The mutation $W^{1175}F$ was introduced using the overlap extension polymerase chain reaction (PCR) method (*25*). PCR was carried out using p72CKD as a template with mutagenic oligonucleotide primers, where the base changes are underlined and italic: 5′-CCTGTA*A*GGT*TT*ATGGCACCGGAG-3′ and 5′-CGGTGCCAT*AA*ACC*T*TAC AGGGAGCAGACC-3′ and wild-type outside primers 5′-TGAGGCTAGCGTCAT-GAAGG-3′ and 5′-CCAGATACCCTCCATCC-3′. The final PCR product was digested and inserted into the shuttle vector pXCKD on unique *Bst*XI and *Stu*I sites. The resulting plasmid pXW1175F also includes a silent mutation in the PCR product (the cDNA encoding amino acid R^{1174} was changed from CGG to AGG) that causes the loss of one *Rsa*I site. The was used to distinguish mutant cDNA from wild-type cDNA. The 1.4 kb *Eco*RI−*Bam*HI fragment from pXW1175F was inserted into the *Eco*RI−*Bam*HI-digested baculovirus transfer vector pVL1392 (Pharmingen) to yield p92W1175F, which was used for baculovirus generation.

The recombinant virus was generated using the BaculoGold kit from Pharmingen. Wild-type and mutant IRKD were expressed in High Five cells (Invitrogen) infected at a multiplicity of infection of 3−5. Forty-eight hours postinfection, cells were harvested. Protein purification was carried out with FPLC (Pharmacia) at 4 °C using three columns in the following order: DEAE 8HR 10 cm × 1 cm (weak anion exchanger, Waters), Superdex-75 Hiload 16/60 (size-exclusion, Pharmacia), and Sepharose Q 8HR 10 cm × 0.5 cm (strong anion exchanger, Waters). Ion exchange columns were developed with linear gradients in NaCl. The buffer used was 50 mM Tris-HCl (pH 7.5) (adjusted at room temperature but used at 4 °C). The purity was confirmed to be at least 98% with ≥5 μg of protein analyzed by SDS−PAGE and Coommassie Brilliant Blue R250 staining. Purified proteins were quantified spectophotometrically at 280 nm (for the unphosphorylated and phosphorylated wild type, $\epsilon = 40\,200\ M^{-1}\ cm^{-1}$, and for $W^{1175}F$, $\epsilon = 32\,000\ M^{-1}\ cm^{-1}$). The purified proteins were stored at −20 °C in 30% glycerol (v/v).

Cytoplasmic Kinase Domain Autophosphorylation and Purification. Wild-type IRKD was autophosphorylated at 25 °C under the following conditions: 2 μM IRKD, 5 mM ATP, 20 mM magnesium acetate, 0.08% hydrogenated Triton X-100, and 1 mM DTT, in 50 mM Tris acetate buffer at pH 7.0 for 1 h. The reaction was quenched with a 3-fold molar excess of EDTA over Mg^{2+}. ATP and ADP concentrations were reduced by four concentration and dilution steps using a Centriprep 30 concentrator (Amicon). The phosphorylated IRKD was repurified using a Sepharose Q 8HR 10 cm × 0.5 cm column using a linear gradient in NaCl. It was determined that the gradient method that was used provided baseline separation of IRKD from phosphorylated IRKD and from any residual ATP and ADP. The final material was analyzed for homogeneity and retention of phosphorylation level (stoichiometry of five phosphates per IRKD) using nondenaturing PAGE with silver stain detection as described previously (*17*), and the concentration was determined spectrophotometrically.

Fluorescence Spectroscopy. Steady state fluorescence emission spectra were obtained with an SLM 4800 spectrofluorimeter operating in the single-photon counting mode. Magic angle polarization conditions were adopted with the excitation polarizer set at 55° and the emission polarizer set at 0° to avoid polarization dependent intensity artifacts. Setting the emission polarizer at 0° was done to minimize the Wood's anomaly of the emission grating. For intrinsic tryptophan fluorescence experiments, an excitation wavelength of 295 nm was used with the excitation and emission slits both set at 8 nm band-pass. Emission spectra were collected over the range of 310−420 nm in 1 nm increments. The final spectra were determined from the average of three spectral scans. All fluorescence experiments were performed at 21 °C. The centroid of the emission spectrum (CES) is the wavelength (λ_c) at which the fluorescence spectrum is divided in two equal areas when plotted on an energy scale (fluorescence vs wavenumber, ν). In practice, $\lambda_c = 1/\nu_c$, such that ν_c divides the area in half in the following equation

$$\int_{\nu_1}^{\nu_c} I(\nu_j)\,d\nu = \int_{\nu_c}^{\nu_2} I(\nu_j)\,d\nu = {}^1/_2 \int_{\nu_1}^{\nu_2} I(\nu_j)\,d\nu \qquad (1)$$

where $I(\nu_j)$ is the fluorescence intensity at wavenumber ν_j.

The total area (right-hand integral) is determined from $\nu_1 = 1/420$ nm to $\nu_2 = 1/310$ nm. The CES of the tryptophan fluorescence provides information about the average environment of all tryptophan fluorescence emitters,[2] the value depending upon the relative quantum yield of fluorescence of each emitter. Fluorescence lifetimes were measured by the time-correlated single-photon counting method as described previously (*26*).

Fluorescence Quenching. Potassium iodide was used as the quenching solute to determine the average accessibility of emissive tryptophans. These experiments were carried out in 50 mM Tris acetate buffer (pH 7.0) with 1 mM DTT. The ionic strength of each sample was kept constant at 0.5 M using potassium chloride, and 0.1 mM sodium thiosulfate was included to inhibit formation of I_3^-. The concentration of IRKD was in the range of 0.3−0.5 μM. Fluorescence instrumentation conditions were as described above. For CES determinations of quenching data, an appropriate blank was subtracted from the emission spectra prior to data reduction. The average solvent accessibility of fluorescent tryptophan residues was characterized in terms of the collisional rate constant, k_q, according to the relationship

$$K_{SV} = k_q \tau_0 \quad (2)$$

where τ_0 is the intensity-weighted mean fluorescence lifetime and K_{SV} is the Stern−Volmer constant. The latter is determined experimentally from measurements of residual fluorescence intensity in the presence of iodide quencher at concentration [Q], as defined by

$$F_0/F = 1 + K_{SV}[Q] \quad (3)$$

where F_0 is the integrated fluorescence intensity in the absence of quencher.

Circular Dichroism Spectroscopy. CD spectra of samples in 0.1 cm path length cuvettes were obtained by using a Jasco J-500A circular dichroism spectrophotometer after calibration with camphorsulfonic acid. The mean residue ellipticity was calculated to be 119.1 on the basis of a molecular mass for IRKD of 48 kDa. Data were collected every 0.5 nm. Spectra were generated from the average of 10 data points per increment. Data were not analyzed below 210 nm due to absorption of the light by GdnHCl and Tris acetate.

Denaturation and Renaturation with GdnHCl. Denaturation experiments were carried out in 50 mM Tris acetate (pH 7.0) with 1 mM DTT. Individual samples of the kinase were prepared for each GdnHCl concentration. An accurate concentration of kinase for the individual samples was maintained by preparing each sample by weight. This required an accurate concentration of stock 6 M GdnHCl which was determined by refractometry, and subsequent dilutions were calculated using the appropriate table of densities. For each GdnHCl dilution, an appropriate blank was also prepared. Samples were left to denature at 24 °C for 16 h in the dark, prior to fluorescence spectroscopy. The fluorescence emission spectrum for each sample and blank was taken using an excitation wavelength of 295 nm and emission over 310−420 nm, and the instrument conditions were as described above. The final emission spectrum for each sample and blank was the average of three spectra. The CES and integrated fluorescence intensity (FI) for each sample were determined after subtraction of the blank. The concentration of GdnHCl in all samples was checked at the end of the experiment by refractometry. These concentrations are reported here to the nearest 0.05 M.

Renaturation experiments were carried out in the same buffer system described above. Apo wild-type IRKD was denatured overnight in either 7, 0.85, or 0.65 M GdnHCl, and individual samples for renaturation were prepared by adding an aliquot of denatured material to vials containing buffer and appropriate concentrations of GdnHCl (0−4 M). Samples were left to renature at 24 °C for 16 h in the dark, prior to fluorescence spectroscopy. Spectra were taken as described above. The concentration of GdnHCl in all samples was checked at the end of the experiment by refractometry.

RESULTS

Denaturation of the Insulin Receptor Kinase Domain. Differences in the inherent conformational stabilities of the apo- and phospho-IRKD were investigated by denaturation in GdnHCl. The fluorescence emission spectra for apo-IRKD at selected GdnHCl concentrations between 0 and 5 M are shown in Figure 1A and for phospho-IRKD in Figure 1B. The excitation at 295 nm allows us to interpret these spectra in terms of tryptophan fluorescence, since tyrosine absorbance is negligible at this wavelength and therefore not a factor in these emission spectra. The net fluorescence intensity (FI) decreases with increasing GdnHCl concentration. When spectra of the IRKD are compared at the extremes (unperturbed vs fully denatured), there is a red shift in the fluorescence observed in apo- and phospho-IRKD. The loss of FI and this spectral shift are expected from the increased level of solvent exposure of previously buried indole rings due to protein unfolding. However, unlike the FI, which decreases more or less steadily, there is a definite blue shift in the emission spectrum at low GdnHCl concentrations, and then the red shift is observed at higher GdnHCl concentrations. For the apo-IRKD, λ_{max}, the wavelength of maximum fluorescence intensity, occurs at 350 nm in the unperturbed state, at 344 nm in the most blue-shifted state at 0.8 M GdnHCl, and at 361 nm in 6 M GdnHCl. For the phospho-IRKD, λ_{max} occurs at 348 nm in the unperturbed state where the FI is 30% lower than in the apo-IRKD. In the most blue-shifted state at 0.55 M GdnHCl, $\lambda_{max} = 344$ nm, and it is 361 nm in 6 M GdnHCl. However, rather than use λ_{max} to characterize the "average" tryptophan environment, we will use the centroid of the emission spectrum (CES) because it is numerically more precise.[2] The calculation of CES is described in Experimental Procedures, and it makes use of the full emission spectrum between 310 and 420 nm.

The complete titration with GdnHCl demonstrates more fully the complex changes of environments experienced by IRKD tryptophans in response to denaturant (Figure 2). The

[2] For simplicity in the initial interpretation of these data, the CES gives an approximation of relative polarity in the environment of an "average" fluorescent tryptophan in the IRKD; blue shifts suggest a greater percentage of the observed fluorescence is from less polar (or more hydrophobic) environments, and red shifts suggest increased contributions from tryptophans in more polar environments. As a point of reference, the CES of *N*-acetyltryptophanamide is 360.6 nm in 20 mM Tris-HCl and 150 mM NaCl (pH 7.4), and it is 360.9 nm in 6 M GdnHCl in the same buffer. The CES has an error of ±0.2 nm, whereas λ_{max} (wavelength of maximum fluorescence intensity) has an error of ±1 nm.

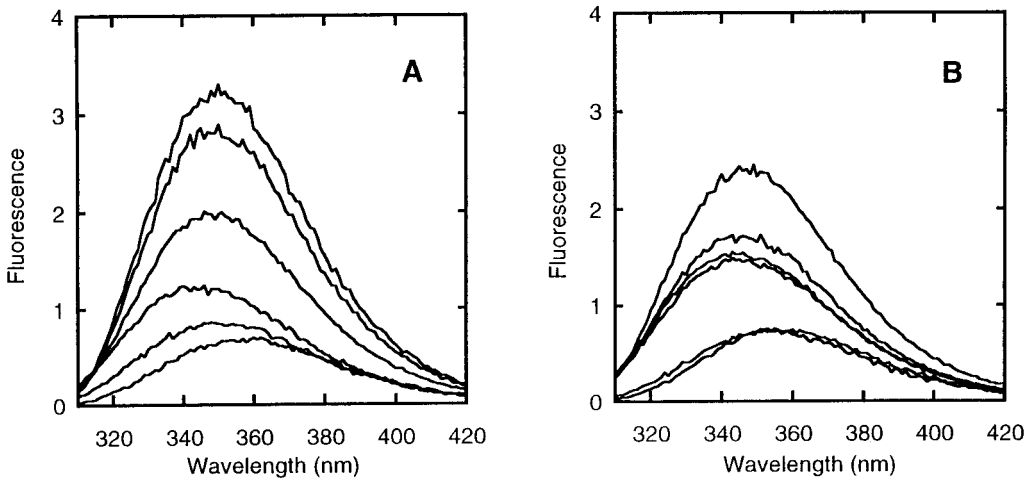

FIGURE 1: Fluorescence emission spectra of IRKD at different GdnHCl concentrations. Spectra were taken at 0.5 μM apo-IRKD (A) and 0.5 μM phospho-IRKD (B), with an excitation wavelength of 295 nm. In both panels, the spectra in descending order correspond to 0, 0.4, 0.8, 1.5, 2.6, and 5.1 M GdnHCl.

shifts in spectral features indicated by the CES (Figure 2A) suggest at least three transitions, and the integrated FI values (Figure 2B) suggest two. There are also significant differences observed between denaturation of the apo-IRKD versus the phospho-IRKD for the first and third transitions, as descibed below. There was no dependence of CES on IRKD concentration between 0.3 and 1.5 μM, which was checked at 0, 0.55, 1.5, 2.5, 4.0, and 6.0 M GdnHCl (not shown). This indicates that none of the spectral changes result from aggregation or oligomerization of the IRKD but arise from changes in the local environments of Trp residues in the monomer.

Transition 1. For the apo-IRKD, there is little if any shift in the CES between 0 and 0.25 M GdnHCl, but a 4.4 nm blue shift from 351.8 to 347.4 nm is observed between 0.25 and 0.8 M GdnHCl. The midpoint of this transition is at 0.65 M GdnHCl. There is a 17% decrease in FI over the range of 0−0.25 M GdnHCl, and a net 67% reduction in FI at 0.85 M GdnHCl. For the phospho-IRKD, the CES is 349.6 nm. Despite this 2.2 nm blue shift with no denaturant, the first transition in CES reaches the same minimum of 347.3 nm. However, the first transition occurs between 0.25 and 0.55 M GdnHCL with the midpoint of the transition at ~0.35 M GdnHCl. The integrated FI of the phospho-IRKD is only 75% of that of the apo-IRKD with no denaturant. The FI decreases with increasing denaturant concentrations, and converges with the FI of the apo-IRKD beginning at ~1.1 M GdnHCl. There appears to be less hindrance to the physical changes underlying this first transition in the phospho-IRKD than in the apo-IRKD, based on these comparisons.

Transition 2. There is a small increase in the CES for the apo-IRKD from 347.4 nm at 0.8 M GdnHCl to 348.2 nm at 0.95 M GdnHCl (Figure 2A). This reversal in the chromatic shift appears as a dip in the CES, but it is not matched by changes in FI (Figure 2B). The same transition in the phospho-IRKD is from 347.3 nm at 0.55 M GdnHCl to 348.2 nm at 0.95 M. The initial and final CES for this transition are the same for apo- and phospho-IRKD, suggesting similar starting and ending conformations for apo- and phospho-IRKD. The lower GdnHCl concentration at the start of this second transition probably results from the apparent loss of

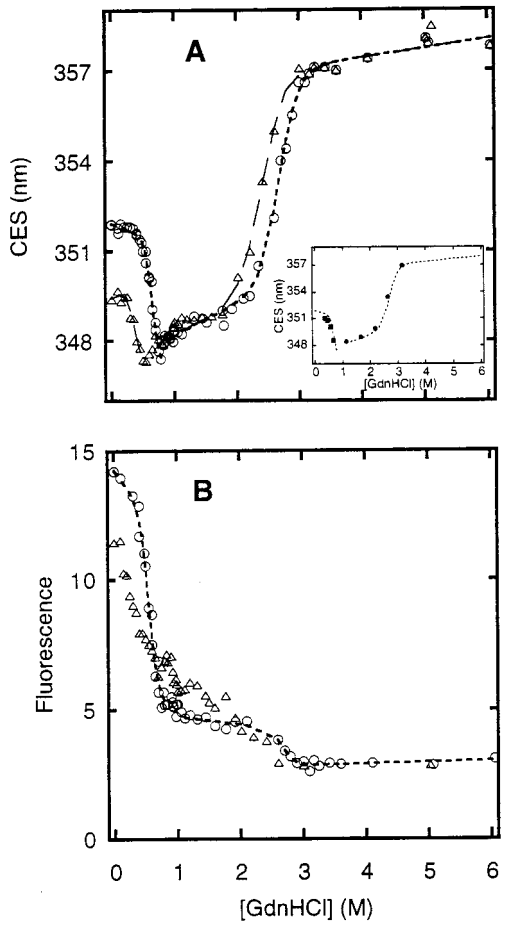

FIGURE 2: Titration of spectral changes of IRKD vs GdnHCl concentration. Denaturation of apo-IRKD (○) and phospho-IRKD (△) was carried out at 0.5 μM protein and monitored by fluorescence. The emission spectra were analyzed for the centroid of the emission spectrum (CES; panel A) and integrated fluorescence intensity (Fluorescence; panel B). Lines show the best fits of data to eq 5 for transitions 1 and 3, as described in the text. The inset shows the renaturation of apo-IRKD. Recovery of CES was determined after denaturation and then dilution to lower GdnHCl concentrations. The apo-IRKD was denatured initially at 7 M GdnHCl (●) or at 0.65 M GdnHCl (■). For comparison, the dashed lines show the best fit of the CES from the denaturation of apo-IRKD (panel A).

stabilization underlying the first phase of denaturation. There was no evidence of aggregation or precipitation of IRKD over transition 2 of the denaturation.

Transition 3. Between the second and third transitions, a slight upward drift in the CES and downward drift in FI are observed with apo- and phospho-IRKD. Over the range of 1.1−1.8 M GdnHCl, the average CES was 348.6 ± 0.3 versus 348.8 ± 0.2 nm, respectively. This intermediate phase probably represents the same states for both apo- and phospho-IRKD. The third transition is between 1.9 and 3.2 M GdnHCl. It covers the large red shift in the CES from ∼349 to ∼358 nm (Figure 2A) and the corresponding small decrease in FI (Figure 2B). While the same transition is observed for both apo- and phospho-IRKD, the midpoints of the third transition also differ, occurring at 2.7 M GdnHCl and 2.4 M GdnHCl for the CES, respectively. Again these findings suggest less inherent stability in the activated state autophosphorylated IRKD than in the basal state apoenzyme.

To extract thermodynamic parameters from these data, we need to show that the transitions are reversibile. Renaturation of apo wild-type IRKD from 7 M GdnHCl shows that the third transition is reversible (Figure 2, inset). However, renaturation to GdnHCl concentrations of less than 1 M is not possible directly from 7 M GdnHCl because the protein precipitates. Renaturation from GdnHCl concentrations of ≥0.9 M, in which the second transitions is appreciable, to GdnHCl concentrations of ≤0.8M is also not observed, and these attempts are accompanied by decreases rather than increases in FI and without recovery of the CES. The loss of FI and an increase in the amount of light scattering indicate aggregation of the IRKD when attempting renaturation across this 0.8 M GdnHCl "barrier", but there was no evidence of aggregation in the "forward" direction of denaturation. Therefore, the second transition appears to be irreversible. However, renaturation of apo-IRKD from 0.65 M GdnHCl is possible, with recovery of the CES and increased FI (Figure 2A, inset). These results demonstrate the reversibility of the first transition. In light of these observations, we used procedures described by Pace and others (*27*−*29*) to fit these denaturation curves (dashed lines). The equations, fitted parameters, and their interpretations will be presented below.

Changes in Secondary Structure. Complete unfolding of a protein is typically characterized by the loss of secondary structure, although some secondary structures may persist at high GdnHCl concentrations (*30*). We monitored the loss of secondary structure by CD over the range of 210−260 nm (Figure 3); shorter wavelengths were not used because of the absorption by GdnHCl and Tris. The molar ellipticity at 222 nm is a frequently reported index of secondary structure, and there were essentially no changes in this parameter at GdnHCl concentrations of ≤1.0 M. However, examination of the CD spectra (Figure 3, inset) indicates that subtle changes in secondary structure could be observed around the midpoint of the first transition as monitored by fluorescence (above). Between 0 and 0.55 M GdnHCl, there are no significant perturbations of secondary structure (curves a and b in the inset of Figure 3). Differences in the CD spectra are evident at 1.0 versus 0.55 M GdnHCl (curve c versus b in the inset of Figure 3). The decrease in [θ] centered around 216 nm could reflect decreased contributions from "unordered" structures, since these have positive values in this region whereas α- and β-structures have negative [θ] values (*31*, *32*). However, the major loss of secondary structure occurs above 1.5 M GdnHCl (curves d and e in the inset of Figure 3). From these observations, we conclude that the third transition observed in the fluorescence experiments (Figure 2; 1.9−3.2 M GdnHCl) is due to complete unfolding of the protein.

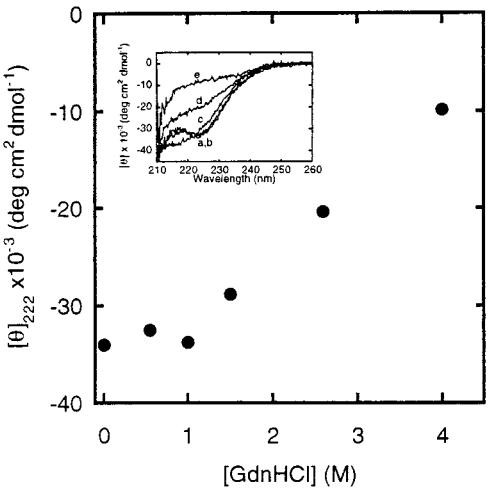

FIGURE 3: Circular dichroism of apo-IRKD. Changes in molar ellipticity at 222 nm ([θ]$_{222}$) were measured at selected GdnHCl concentrations. The inset shows the CD spectra at these selected GdnHCl concentrations: (a) 0, (b) 0.55, (c) 1.0, (d) 2.6, and (e) 4.0 M.

The first and third transitions are well-separated in GdnHCl concentration. Unlike the third transition in the denaturation profiles, the first transition does not appear to involve major changes in secondary structure, and is observed at very low GdnHCl concentrations in both apo- and phospho-IRKD. The first transition also appears to be more sensitive to the autophosphorylation state of the IRKD, and if it is dominated by changes in the local environment of a single tryptophan would provide an excellent probe for the dynamics of phosphorylation-related conformational changes. Therefore, to gain further insight into the origins of the first transition, we employed site-directed mutagenesis.

Spectral Properties and Denaturation of W^{1175}F-IRKD. Using files from the Brookhaven Protein Data Bank (1IRK and 1IR3), we examined differences in solvent exposure and polar residues near the indole rings of tryptophans in the conserved catalytic core. In general, there are few changes in side chains around the indole rings, other than near W^{989} and W^{1175}. W^{989} is the most solvent-exposed in both the apo- and phospho-IRKD core structures, and the relative extent of exposure is not dramatically different in these two structures. However, W^{1175} is virually inaccessible to solvent in the apo-IRKD core structure, but it becomes substantially more solvent-exposed in the tris-phosphorylated core if the peptide substrate is removed from the structure (see Discussion). Empirically, the substitution of Phe for W^{989} does not shift the CES of the fluorescence emission spectrum (not shown), suggesting that it is not the primary red-shifted emitter of the IRKD that is quenched over the first transition. The same substitution of Phe for W^{1175} yields a CES of 345.5 nm and a kinase domain with only 25% of the FI of the wild-type apo-IRKD, measured at identical concentrations[3] as shown in Figure 4. Therefore, W^{1175} has an emission spectrum that is red-shifted, compared to that of the native

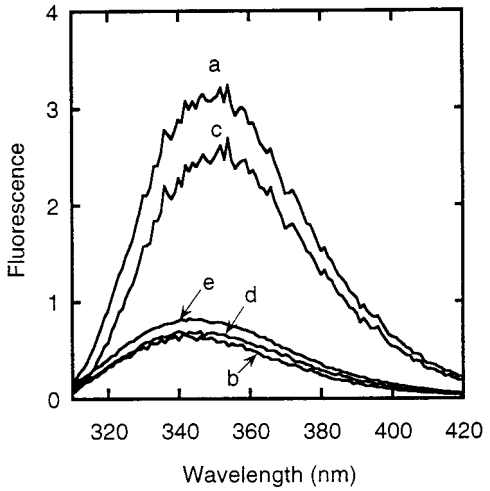

FIGURE 4: Characterization of $W^{1175}F$ mutant IRKD. Fluorescence emission spectra are shown for the wild-type apo-IRKD (a; CES = 351.8 nm) and apo-$W^{1175}F$ (b; CES = 346.2 nm) in their unperturbed states (buffer only, zero denaturant). The difference spectrum represents the emission characteristic of W^{1175} (c; spectrum a minus spectrum b; CES = 353.3 nm). Comparison of spectrum b with the spectrum for the denaturation of wild-type IRKD shows the loss of FI and the largest observed blue shifts in the CES; spectra for wild-type apo-IRKD at 0.8 M GdnHCl (d; CES = 347.4 nm) and for phospho-IRKD in 0.55 M GdnHCl (e; CES = 347.3 nm) are shown. All spectra were taken using 0.5 μM kinase domain.

IRKD; from the difference spectrum, W^{1175} has a calculated CES of 353.3 nm (curve c of Figure 4). The fluorescence spectrum of the $W^{1175}F$ mutant is similar to that of wild-type apo-IRKD at 0.8 M GdnHCl and phospho-IRKD at 0.55 M GdnHCl (curves d and e of Figure 4). Together, these data support the conclusion that W^{1175} is in a strongly polar environment and is the main contributor to the tryptophan fluorescence emission spectrum of the wild-type kinase.

Denaturation of $W^{1175}F$ in GdnHCl is shown in Figure 5 along with the best-fit lines for the first and third transitions of the wild-type apo- and phospho-IRKD. The first transition reported by the blue-shifted CES of the wild-type IRKD is now absent. The second transition involving the red shift around 0.8 M GdnHCl is more apparent. The drift in the CES and FI between 1.1 and 1.8 M GdnHCl has approximately the same slopes as observed for the wild-type apo-IRKD. The third transition appears to overlap that of the wild-type apo-IRKD as well; the midpoint of this transition is at 2.7 M GdnHCl. At 6 M GdnHCl, the integrated fluorescence intensity for $W^{1175}F$ is $^4/_5$ of that of wild-type apo- and phospho- IRKD, as would be expected for a protein containing four versus five tryptophans (assuming that all emitting tryptophans are in identical environments in the fully denatured state). Comparison of the denaturation profile of the $W^{1175}F$ mutant to the wild-type best-fit lines suggests that there is residual emission from W^{1175} contributing to the spectral characteristics over the second and third transitions. The gradual rise in the CES

[3] The $W^{1175}F$ mutant IRKD, used to obtain the difference spectrum in this work, shows a basal level of peptide phosphorylation activity. However, when autoactivation was analyzed at 2 μM IRKD, 5 mM ATP, 20 mM magnesium acetate, and 50 mM Tris acetate (pH 7.0), the wild-type IRKD, but not the $W^{1175}F$ mutant, shows a 200-fold increased kinase activity (S. M. Bishop and R. A. Kohanski, unpublished observations). The basis for this difference will be explored in future studies.

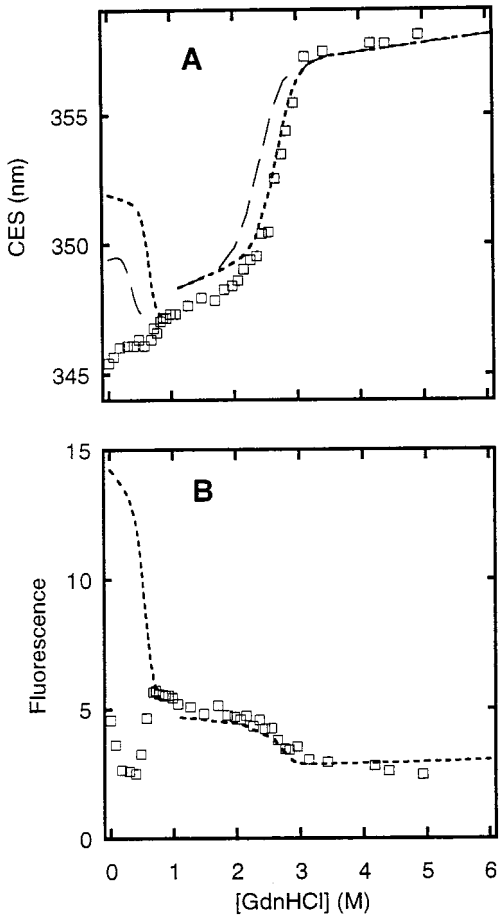

FIGURE 5: GdnHCl denaturation of $W^{1175}F$. The denaturation of $W^{1175}F$ mutant apo-IRKD (□) was assessed at 0.5 μM kinase domain, and the fluorescence emission spectra were characterized as described in the legend of Figure 2. For comparison, best fits for wild-type apo-IRKD (short-dash line) and phospho-IRKD (long-dash line) from Figure 2 are shown for the CES (A) and for apo-IRKD fluorescence intensity (B).

over the range of 1.1−1.8 M GdnHCl for the $W^{1175}F$ mutant is ~1 nm lower than for the wild-type IRKD, although the slope is virtually the same (Figure 5A). The minimum in the CES of wild-type IRKD from the first transition in denaturation is ~1 nm above the "baseline" value of 364.0−364.4 nm observed for the $W^{1175}F$ mutant (0.2−0.5 M GdnHCl). This baseline and the 1 nm offset are used to analyze denaturation of apo- and phospho-IRKD, as described below.

Thermodynamic Parameters from the Denaturation Profiles. The denaturation curves followed by the CES or FI show multiple linear and nonlinear regions (Figures 2 and 5). The nonlinear phases indicate cooperative transitions and reflect unfolding events (if denaturation is reversible) because protein folding is a cooperative process. The inherent conformational stability of a protein (ΔG_{H_2O}) can therefore be estimated from the unfolding characteristics of the cooperative transitions (*27*). The free energy of unfolding is estimated by assuming a minimal two-state transition between states "a" and "b". State a is usually the native (unperturbed) state, and b is an intermediate or fully denatured state. Each such transition is characterized by a midpoint concentration of denaturant ($[D_{ab}]_{0.5}$) and a denaturant index (m_{ab}) which indicates the relative cooperativity of that denaturant-induced unfolding process (m_{ab} is the slope

Table 1: Conformational Stabilities and Transition Midpoints from GdnHCl Denaturation[a]

	transition 1		transition 3		
parameter	apo-WT	phospho-WT	apo-WT	phospho-WT	$W^{1175}F$
$-\Delta G_{H_2O}$ (kcal/mol)	5.2 ± 1.9	2.8 ± 1.3	8.9 ± 1.7	7.4 ± 2.0	9.5 ± 1.2
$-m_{ab}$ (kcal M^{-1} mol^{-1})	7.8 ± 1.6	7.0 ± 1.2	3.3 ± 1.6	3.1 ± 1.9	3.4 ± 1.1
$[D_{ab}]_{0.5}$ (M)	0.65 ± 0.25	0.40 ± 0.06	2.7 ± 0.1	2.4 ± 0.1	2.8 ± 0.1

[a] Values (±1 SD) were calculated from the CES data for wild-type IRKD (WT; Figure 2A) and the $W^{1175}F$ mutant IRKD ($W^{1175}F$; Figure 5A), using eqs 4 and 5.

of a plot derived from logarithmic transformation of the data across the cooperative transition; see Figure 2 of ref *29*). Together, these provide the free energy inherent in the protein with no denaturant (*28*):

$$\Delta G_{H_2O} = m_{ab}[D_{ab}]_{0.5} \quad (4)$$

which is referred to as the free energy of unfolding or of denaturation. To obtain values for m_{ab} and $[D_{ab}]_{0.5}$, we used nonlinear least-squares fitting of the data for transitions 1 and 3, treated as independent events, according to the method of Santoro and Bolen (*29*) and using a form of the equation given by Scholtz (cf. eq 11 of ref *28*):

$$Par_{obs} = \{Par_a + m_a[D] + [Par_b + m_b[D] \exp(m_{ab}([D] - [D_{ab}]_{0.5})/RT]\}/\{1 + \exp[m_{ab}([D] - [D_{ab}]_{0.5})/RT]\} \quad (5)$$

where Par_{obs} is the observed fluorescence parameter (CES or FI) which changes with the concentration of denaturant [D]. The cooperative a-to-b transition is preceded by approximately linear changes in Par_{obs} with a slope m_a and followed by a change with a slope m_b, where these are slopes on the primary plot of the denaturation profile. The data over the preceding and following phases, when extrapolated to zero denaturant, give values Par_a and Par_b, respectively. These slopes and intercepts for the two linear terms of the equation (Par and m[D]) were obtained by linear regression.[4] Nonlinear regression was used to fit data between the linear phases and to generate the best-fit lines in Figure 2. Fitting of the FI versus GdnHCl concentration was successful for the apo-IRKD but unreliable for the phospho-IRKD and the $W^{1175}F$ mutant. Therefore, we will rely on parameters from the CES data (Table 1).

[4] For transition 1, the CES with no denaturant was used as Par_a (351.8 and 349.6 nm for apo- and phospho-IRKD, respectively). For both states of the kinase, a Par_b of 346.3 nm was used, an m_a of −0.17 nm/M and an m_b of 0.33 nm/M were used, where m_b was the slope taken from the $W^{1175}F$ denaturation between 0.2 and 0.7 M GdnHCl (Figure 5), and Par_b was the intercept from these data to which a 1 nm offset was added to account for the partial quenching of W^{1175} in the wild-type kinase, as described in the text. These numbers use the assumption that a common state was reached after transition 1, but the initial states differed, as indicated by the difference in CES with no denaturant. Nonlinear regression was carried out using CES data between 0.3 and 0.8 M GdnHCl for the apo-IRKD and between 0.1 and 0.5 M GdnHCl for the phospho-IRKD. Similarly, we interpret the data to indicate that the state between the second and third transition (1.1−1.8 M GdnHCl) and after the third transition was the same for both apo- and phospho-IRKD. Therefore, an average slope and intercept were calculated by linear regression for the combined CES data between 1.1 and 1.8 M GdnHCl to give a Par_a of 348.0 nm and an m_a of 0.55 nm/M preceding transition 3, and a Par_b of 356.2 nm and an m_b of 0.39 nm/M for the linear phase following transition 3. Data used for the nonlinear regression over transition 3 were from the range between 1.7 and 3.3 M GdnHCl for both apo-IRKD and phospho-IRKD.

The free energy of unfolding is lower for the phospho-IRKD than for the apo-IRKD. This difference amounts to ~2.3 and ~1.5 kcal/mol for the first and third reversible transitions, respectively, and indicates that phosphorylation reduces the stability of the IRKD. Also, ΔG_{H_2O} is lower for the first transition than for the third. This suggests the first transition involves fewer residues and interactions than the third transition, which entails complete unfolding of the kinase domain (based on the CD spectra, Figure 3). However, the irreversible nature of transition 2 might preclude summing the free energies of transitions 1 and 3, because these are based on extrapolation to zero denaturant (*27*). It is not clear that extrapolation to zero denaturant over the third transition leads to a native "ground state" rather than an intermediate "ground state" that we know is not in equilibrium with the unperturbed structure (based on renaturation data, inset of Figure 2). However, that intermediate appears to be the same for both apo- and phospho-IRKD, so comparison of the calculated free energies of unfolding over transition 3 is reasonable. These values (Table 1) are similar to or somewhat higher than others reported for global unfolding at about the same temperature, e.g., 7.8 kcal/mol for the unfolding of mitochondrial creatine kinase (*33*) or ~9 kcal/mol for α-chymotrypsin (*34*). Global unfolding of the $W^{1175}F$ mutant IRKD is only ~0.7 kcal/mol more stable than the wild-type apo-IRKD, which is probably not a significant difference. In an exhaustive study requiring 11 Trp-to-Phe and/or Phe- and Tyr-to-Trp substitutions, Steer and Merrill (*35*) found that these changes did not in themselves perturb the native structure or global unfolding mechanism. Similarly, we find that the Phe-for-Trp substitution did not disrupt folding, by inference from the small effect of this mutation on unfolding.[3] However, Steer and Merrill replaced and added tryptophans as fluorescent reporters of denaturation in different regions of their protein. In our study, we have removed one reporter. This single-Trp replacement strategy was necessary to show that W^{1175} is the major fluorophore of the wild-type IRKD, and it also allowed us to identify the region influenced by the denaturant within a specific GdnHCl concentration range. This approach also showed that W^{1175} fluorescence probably contributes to the signal over transition 3. Therefore, in future studies it will be necessary to probe the contributions of Trp residues to global stabilization with nonfluorescent techniques.

Fluorescence Quenching. In addition to these conclusions based on fitting of the denaturation data to eq 5, we can take advantage of the fact that W^{1175} is positioned in the active site. This, its dominance of the unperturbed emission spectrum, and the >2 nm decrease in the CES associated with autophosphorylation, suggest that it might also report changes in solvent accessibility in the catalytic cleft. To test this hypothesis, quenching of tryptophan fluorescence by

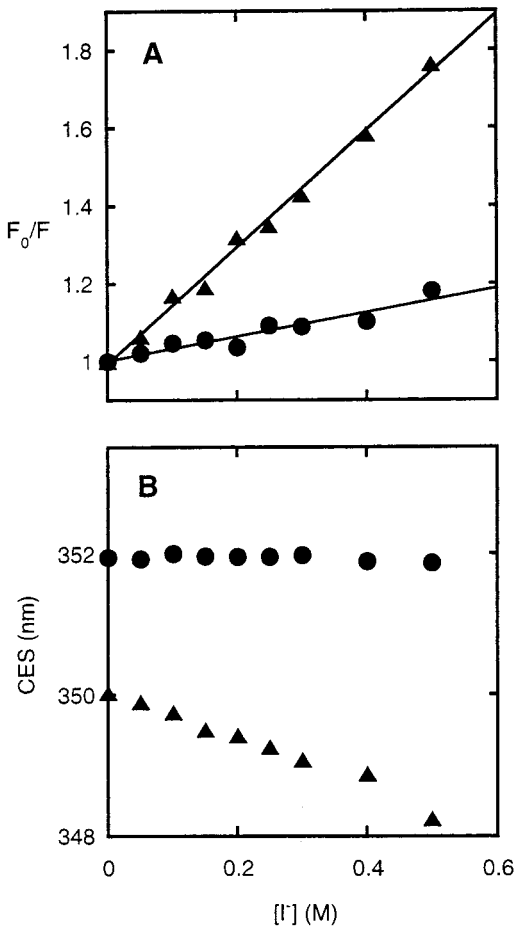

FIGURE 6: Iodide quenching of IRKD fluorescence. Quenching of fluorescence of wild-type apo-IRKD (●) and phospho-IRKD (▲) was carried out at a constant ionic strength and 0.5 μM kinase domain. The integrated fluorescence intensity over 310−420 nm was used, after subtraction of the background spectrum. (A) Stern−Volmer plot of the extent of relative quenching vs iodide concentration. (B) Change in the CES vs iodide concentration.

iodide was carried out for apo- and phospho-IRKD without denaturant. The results are shown as a Stern−Volmer plot in Figure 6. There is very little quenching observed for the apo-IRKD in contrast to the phospho-IRKD, indicated by the respective Stern−Volmer constants of 0.3 and 1.5 M^{-1}. To conclude that a change in solvent accessibility occurred, we determined the intensity-weighted mean fluorescence lifetime, τ_0, and the collisional rate constant, k_q, was calculated from K_{SV} using eq 2; k_q is the parameter dependent on relative solvent accessibility (*19*).The intensity-weighted mean lifetime for apo-IRKD is 7.0 ns and for phosphorylated IRKD is 7.4 ns. These yield collisional rate constants of 4.3 $\times 10^7$ and 20.3 $\times 10^7$ M^{-1} s^{-1}, respectively. For comparison, the diffusion limit is $\sim 5 \times 10^9$ M^{-1} s^{-1} for unhindered access of an indole ring to iodide in aqueous solution (*21*). The observed 5-fold increase in K_{SV} (or k_q) could arise from the greater level of exposure of at least one fluorophore in the protein. Analysis of the CES versus concentration profile of iodide quencher shows virtually no change upon quenching in the apo-IRKD (Figure 6B). However, a decrease with increasing quencher concentration is observed with the phospho-IRKD. This quencher-induced blue shift of the emission spectrum is consistent with increased level of solute quenching of a more solvent-exposed W^{1175} in the activated, gate-open conformation of the IRKD.

DISCUSSION

There is a 200−500-fold increase in the catalytic efficiency of both the native insulin receptor and the recombinant cytoplasmic kinase domain upon autophosphorylation (*12*, *36*, *37*). The principal steric barrier to substrate phosphorylation is the activation loop which rests within and across the catalytic cleft of the apoenzyme (*15*). This gate-closed conformation is the structural basis for the weak metal−ATP and peptide substrate interactions in the basal state, indicated by Michaelis constants that are ≥1 mM (*17*). The autophosphorylated IRKD core with a peptide substrate and metal−ATP analogue bound shows the AL swung away from the active site into a gate-open conformation that is stabilized by new interactions (*16*). Those between AL phosphotyrosines and neighboring arginines within the AL itself are especially important because the enzyme cannot be fully activated without AL phosphorylation (*13*). Hubbard also described rotation of the small lobe toward the large lobe; the β-sheet comprising most of the small lobe realigned as an approximately rigid unit, whereas helix αC changed its orientation on the surface of the small lobe. As in other protein kinases, the orientation of this helix is linked to efficient binding of the metal−ATP complex (*38*−*43*). Except for the activation loop itself (D^{1150}−P^{1172}), there are very few perturbations in the large lobe. These IRKD core structures present an elegant description of kinase activation, principally in terms of steric hindrance and its relief. The observed lobe rotations also demonstrate flexibility within the IRKD catalytic core, and this is potentially relevant to catalytic cycling. Williams et al. (*44*) point out, however, that lobe rotation and cleft closed and opened conformations, per se, do not necessarily define the active versus the "inactive" states. This follows logically from inferences stated by Xu et al. (*41*) and Sicheri et al. (*42*) that restriction of the catalytic core's mobility by itself may be sufficient to inhibit catalysis without intrasteric inhibition at the active site. Moreover, steady state kinetics requires at least two stable "active" conformations in a catalytic cycle: the enzyme with and without substrate(s) bound.

In this context, we sought to analyze the inherent conformational stability of the insulin receptor's kinase domain as a function of its phosphorylation state. We approached this problem through intrinsic fluorescence because the four tryptophan residues buried within the large lobe are conserved in protein tyrosine kinases (*45*); W^{1200} of the IRKD is variable in Src and JAK/Tyk families and should contribute to structural stabilization. In contrast, tryptophan residues of the small lobe are variable in number, are less conserved spatially, and are all more solvent-exposed. In concert with other exposed hydrophobic residues, these may form surface binding sites with regulatory importance, as appears to be the case for Src family kinases (*44*) and certainly for CamKI (*46*, *47*).

Structural Origins of the Denaturation Profiles. It is of interest to determine if autophosphorylation alters the stability of one lobe more so than the other, because this would have implications for the conformational change during catalysis. At this point, however, we cannot conclude that the small lobe is less (or more) stable than the large lobe of the IRKD. Also, we do not know the extent of thermodynamic linkage between them. We have found that the first transition is well-

separated in GdnHCl concentration from the third. However, we cannot infer from this observation whether the small and large lobes denature independently because we cannot yet assign a specific region of the denaturation curve to the loss of β-sheet structure; the small lobe has most of the β-sheet of the core. In fact, the CD results do not support a loss of β-sheet over the first transition. This is unlike the GdnHCl- or urea-induced denaturation of creatine kinase, which also displays a complex unfolding pathway (*33*) but where there appears to be a single unfolding intermediate state and therefore probably strong linkage between its two domains. In the case of the IRKD, there is no indication that W^{989} has emission characteristics that can be resolved from the overall spectrum and which would aid in monitoring unfolding of the small lobe using fluorescence. In contrast, the intrinsic fluorescence *is* dominated by W^{1175}, and therefore, we have an endogenous probe reporting from the catalytic cleft on local conformational changes. However, the actual photophysical mechanism(s) underlying W^{1175} quenching over transition 1, as well as the identities and possible roles of neighboring side chains, are not known. Furthermore, the active site forms only part of the local environment of W^{1175}. Therefore, we can infer a structural dependence of transition 1 on the catalytic cleft, based on the observed quenching. Also, the difference between the phospho- and apo-IRKD denaturation profiles suggests an influence of the activation loop conformation and/or phosphorylation state. There may be contributions from the juxtamembrane or carboxy-terminal phosphorylations as well, which can be analyzed in future studies with these methods.

The second transition involves an irreversible change. The crystal structure of the apo-IRKD core (*15*) shows one cis-prolyl residue, P^{1071}, which could interfere with refolding. However, there are multiple prolines in the IRKD, many of which are outside of the core and which could contribute to the irreversibility of transition 2. The third transition is reversible and arises from global unfolding of the protein, as indicated by the red-shifted CES, the drop in FI, and the CD spectra. We anticipate that this transition will be especially informative about the effects of core-flanking regions on the IRKD core's stability (S. M. Bishop and R. A. Kohanski, work in progress).

Relationship between Stability and Function. The 200−500-fold increase in catalytic efficiency translates into 2.9−3.4 kcal/mol of free energy that is available in the activated state that is lacking in the basal state. The denaturation data presented here indicate that the free energy difference could originate from the decrease in the level of stabilization of the protein structure which accompanies autophosphorylation of the IRKD (Table 1). The free energy changes in the two transitions show 2.3 kcal/mol reported from the catalytic cleft region (via the fluorescence of W^{1175} over transition 1) and 1.5 kcal/mol from complete unfolding (transition 3). Either or both transitions could be thermodynamically linked to activation since both are influenced by autophosphorylation.

A further context for understanding the issue of possible thermodynamic linkage between catalysis and denaturation can be found in other studies on the relationships among phosphorylation, stability, and function. Two proteins in the phosphoenolpyruvate:sugar transport system of *Bacillus subtilis* were each found to become destabilized by histidine phosphorylation. That phosphoryl group could be transferred from the phosphohistidine residue, and therefore, destabilization may reflect its position in the pathway as a catalytic intermediate (*48*). Scholtz and colleagues (*49, 50*) suggested that phosphorylation at a regulatory serine increased slightly the stability of HPr. However, through mutagenesis they showed there was little detectable coupling between the regulatory and transferable phosphorylation sites (*49*). The small increase in stability (0.7 kcal/mol) from regulatory Ser phosphorylation was not enough to account for the decrease in phosphorylation of the "catalytic" histidine (100-fold drop, or ~2.5 kcal/mol). Together, these support a regulatory mechanism dependent on electrostatic and steric factors rather than on thermodynamic coupling of intrinsic conformational stabilities. Nosworthy et al. (*48*) extended these observations to the thermal denaturation of Enzyme I, the phosphoryl donor for HPr (*51*). They demonstrated that phosphorylation of the amino-terminal domain promoted its destabilization so that thermal denaturation both was less cooperative (less coupled to the carboxy-terminal domain) and occurred at a lower temperature than that of the apoprotein. The carboxy-terminal domain has a function in dimerization and in the ability of the amino-terminal domain to become phosphorylated by phosphoenolpyruvate at the beginning of the regulatory chain. Therefore, in summarizing their work and that of others, they propose that destabilization in Enzyme I could account for the directionality of phosphoryl transfer and thus of regulation in that transport system.

Both principles may apply to the activation of the IRKD. Steric factors clearly are important in substrate access to the catalytic cleft. However, our data suggest that thermodynamic factors mediated by the phosphorylation state could be significant. The free energy differences observed by denaturation (2.3 and 1.5 kcal/mol) and the relative catalytic efficiency (~3 kcal/mol) may be a byproduct of the need to promote (or avoid) other regulatory binding interactions associated with IRKD autophosphorylation. However, it is also possible that the lower inherent stability is more permissive of conformational changes that would be required for a full catalytic cycle. This may apply more to metal−ATP binding because there are more changes in the adenine binding pocket itself than among residues involved directly in peptide substrate binding and which are largely on the surface. The crystal structure of the tris-phosphorylated IRKD core was determined as a ternary complex, with ATP analogue and peptide substrate (*16*), and the apoprotein was crystallized without these ligands (*15*); the binding sites were occupied intrasterically by residues of the AL. The average *B*-value for bonded atoms in the phospho-IRKD core was significantly lower than the *B*-value for the apo-IRKD core (18.5 $Å^2$ compared to 22.3 $Å^2$, for essentially the same *R*-values). This indicates much less average disorder in the phospho-IRKD core, but we cannot distinguish the contributions of autophosphorylation from those of substrate binding to "fixing" the observed conformation in the crystal structure. However, we propose that the lower stability inherent in the conformation of the phospho-IRKD could facilitate substrate binding and conformational changes which are expected to occur during a catalytic cycle.

Conformational Change Resulting from Autophosphorylation Reported by Intrinsic Fluorescence and Iodide Quenching. In the unperturbed state (with no denaturant), there is a >2 nm drop in the CES associated with autophosphorylation.

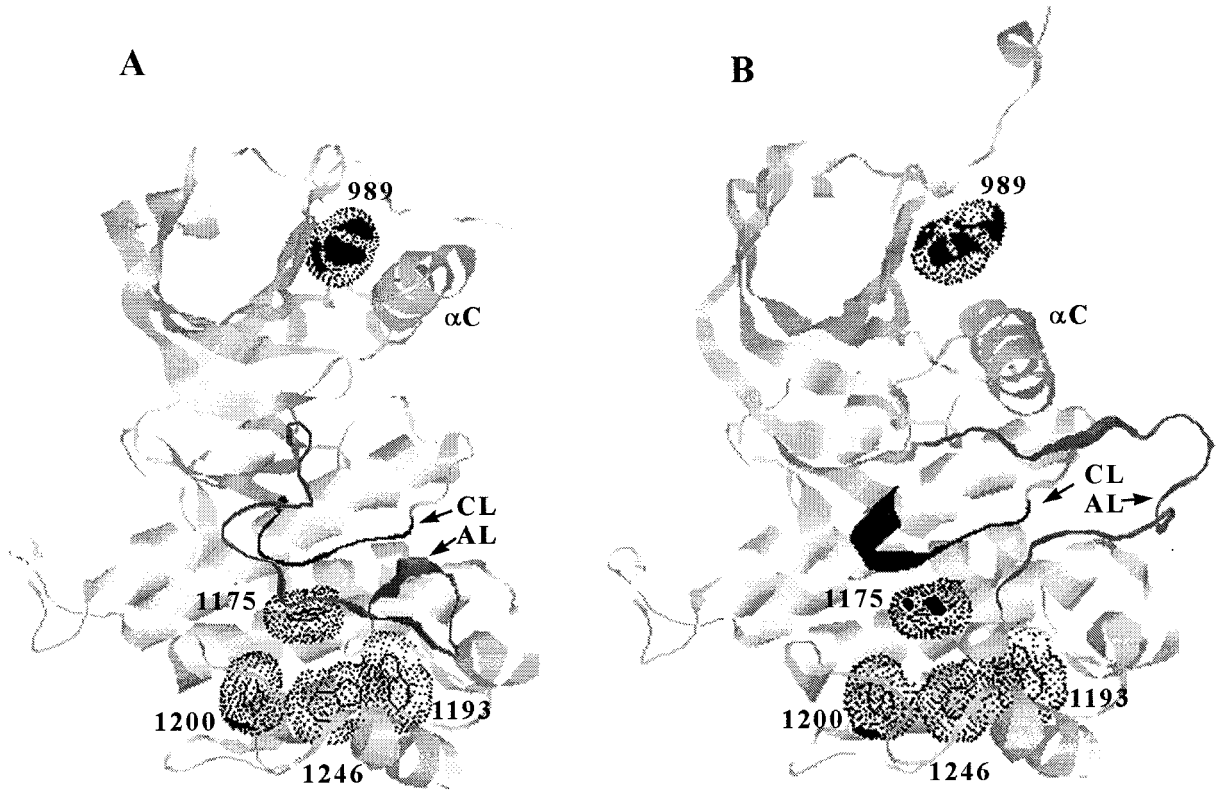

FIGURE 7: Accessibility of tryptophans in the IRKD core. Ribbon diagrams of the apo-IRKD core (A) and tris-phosphorylated IRKD-core (B) are shown. Each large lobe is in approximately the same orientation. Indole rings of the five tryptophan residues (numbered) are depicted as wireframes inside dot surfaces showing their hard sphere volumes. The surfaces of each indole ring accessible to a 2.2 Å sphere were determined by the RasMol (*53*) commands "set solvent true" and "set radius 2.2" after the coordinate files were modified (below). These surfaces are shown as black patches on W^{989} and W^{1200} in panel A and on W^{989}, W^{1175}, and W^{1200} in panel B. Features of the IRKD mentioned in the text are marked on the figures: **αC**, helix αC ($L^{1038}-M^{1051}$); **CL**, catalytic loop (black, $R^{1131}-N^{1137}$); and **AL**, activation loop (dark gray, $D^{1150}-P^{1172}$). The orientation in panel A shows the **AL** crossing in front of the **CL** and W^{1175}, the gate-closed and cleft-open conformations, vs the **AL** swung away from the catalytic center and exposing the **CL** and part of W^{1175} in panel B, the gate-open and cleft-closed conformations. Brookhaven Protein Data Bank files 1IRK and 1IR3 were used. The coordinate files were modified as follows. Water and nonbonded heteroatoms were removed from both files; IRK3 was reduced from the "dimer" to the "monomer" IRKD core polypeptide, and "ANP" and peptide substrate were removed as well. The figure was assembled and labeled using Adobe Photoshop.

This can be explained by quenching of W^{1175} fluorescence in the phospho-IRKD. There are at least four mechanisms by which quenching could depend on the orientations of specific neighboring amino acid side chains or amide bonds of the peptide backbone (*52*). Solvent quenching is one of these mechanisms. In Figure 7, we show the differences in the solvent accessibility of tryptophans' indole rings in the apo- and phospho-IRKD core, analyzed according to the two crystal structures. In the apo-IRKD core structure, access of a 2.2 Å radius sphere (iodide) is largely confined to a small area on the surface of W^{1200} in the large lobe and to ~10% of the surface of W^{989} in the small lobe (Figure 7A). On the basis of this extensively exposed surface, we might have expected substantial quenching if W^{989} had been a strong fluorescence emitter. Therefore, since little iodide quenching was observed in the apo-IRKD, this either confirms that W^{989} is a weak emitter to a nonemitter or suggests that one of the core-flanking regions (not present in the crystal structures) blocks solute access. The areas of these two indole rings that are accessible to water, estimated with a 1.2 Å radius sphere, are about 2−3-fold greater than those areas exposed to iodide. Although eight water molecules appear in the crystal structure near the indole ring of W^{1175}, this side chain is not accessible to a 2.2 Å sphere even after those water molecules are edited out of the structure. This inaccessibility is entirely consistent with the virtual absence of fluorescence quenching by iodide in the basal state. Because of the dominance of W^{1175} and its location in the catalytic cleft, it suggests strongly that a gate-closed conformer, as observed in the crystal structure, predominates in solution. This is depicted in Figure 7A, with a segment of the AL obscuring that part of the W^{1175} indole ring that will become exposed, as indicated in Figure 7B.

Accessibility in the activated state changes very little for W^{1200} but increases significantly for W^{1175}. Factors such as the presence of nearby charges can significantly alter iodide quenching of otherwise fully exposed indole rings, where the diffusion-limited rate of quenching would be $\sim 5 \times 10^9$ M^{-1} s^{-1} (*21*). The quenching rate constants for the IRKD are 25−100-fold lower. In the case of W^{1200}, it is quite possible that local electrostatic effects reduce the level of iodide quenching, because there are three carboxylic acid side chains around the water-accessible surface. In addition, and as illustrated in Figure 7, limited steric access should contribute to the low quenching rate constants since only a few percent of the net surface areas of W^{1200} and W^{1175} indole rings are exposed to iodide.

Summary. Previous mutagenic, kinetic, and structural studies cited above have implied or shown directly that autophosphorylation of the insulin receptor and its recombinant kinase domain changed the conformation of the activation loop. The denaturation experiments presented here

demonstrate that autophosphorylation lowers the conformational free energy of the enzyme. Mutagenesis and iodide quenching showed that W^{1175}, in the catalytic cleft, is the major reporter of conformational change. These studies provide baseline fluorescence parameters that will advance kinetic and equilibrium studies of substrate binding, as well as their dependence and impact on conformation. Because of the conservation of large lobe tryptophans, and especially of W^{1175}, such investigations should be feasible with other protein tyrosine kinases.

ACKNOWLEDGMENT

We thank Qing-Xiang Wei for subcloning and expression of the W^{1175}F mutant and William Laws, Elena Rusinova, Natalia Rodinova, and Ed Rachofsky for advice and helpful discussions throughout the course of this work. We particularly thank Steven Hubbard for making coordinate files of his crystal structures available prior to release from the Brookhaven Protein Data Bank.

REFERENCES

1. Lane, M. D., Ronnett, G. V., Kohanski, R. A., and Simpson, T. L. (1985) *Curr. Top. Cell Regul. 27*, 279−292.
2. Kasuga, M., Fujita Yamaguchi, Y., Blithe, D. L., and Kahn, C. R. (1983) *Proc. Natl. Acad. Sci. U.S.A. 80*, 2137−2141.
3. White, M. F., and Kahn, C. R. (1994) *J. Biol. Chem. 269*, 1−4.
4. Villalba, M., Wente, S. R., Russell, D. S., Ahn, J. C., Reichelderfer, C. F., and Rosen, O. M. (1989) *Proc. Natl. Acad. Sci. U.S.A. 86*, 7848−7852.
5. Ebina, Y., Ellis, L., Jarnagin, K., Edery, M., Graf, L., Clauser, E., Ou, J., Masiarz, F., Kan, Y. W., Goldfine, I. D., Roth, R. A., and Rutter, W. J. (1985) *Cell 40*, 747−758.
6. Tornqvist, H. E., Pierce, M. W., Frackelton, A. R., Nemenoff, R. A., and Avruch, J. (1987) *J. Biol. Chem. 262*, 10212−10219.
7. Tavare, J. M., and Denton, R. M. (1988) *Biochem. J. 252*, 607−615.
8. Tornqvist, H. E., Gunsalus, J. R., Nemenoff, R. A., Frackelton, A. R., Pierce, M. W., and Avruch, J. (1988) *J. Biol. Chem. 263*, 350−359.
9. Feener, E. P., Backer, J. M., King, G. L., Wilden, P. A., Sun, X. J., Kahn, C. R., and White, M. F. (1993) *J. Biol. Chem. 268*, 11256−11264.
10. Kohanski, R. A. (1993) *Biochemistry 32*, 5773−5780.
11. Ellis, L., Clauser, E., Morgan, D. O., Edery, M., Roth, R. A., and Rutter, W. J. (1986) *Cell 45*, 721−732.
12. Flores Riveros, J. R., Sibley, E., Kastelic, T., and Lane, M. D. (1989) *J. Biol. Chem. 264*, 21557−21572.
13. Zhang, B., Tavare, J. M., Ellis, L., and Roth, R. A. (1991) *J. Biol. Chem. 266*, 990−996.
14. Murakami, M. S., and Rosen, O. M. (1991) *J. Biol. Chem. 266*, 22653−22660.
15. Hubbard, S. R., Wei, L., Ellis, L., and Hendrickson, W. A. (1994) *Nature 372*, 746−754.
16. Hubbard, S. R. (1997) *EMBO J. 16*, 5572−5581.
17. Cann, A. D., Bishop, S. M., Ablooglu, A. J., and Kohanski, R. A. (1998) *Biochemistry 37*, 11289−11300.
18. Eftink, M. R. (1994) *Biophys. J. 66*, 482−501.
19. Eftink, M. R., and Ghiron, C. A. (1976) *Biochemistry 15*, 672−680.
20. Eftink, M. R., and Ghiron, C. A. (1981) *Anal. Biochem. 114*, 199−227.
21. Lehrer, S. S. (1971) *Biochemistry 10*, 3254−3263.
22. Lakowicz, J. R. (1983) in *Principles of Fluorescence Spectroscopy*, Plenum Press, New York.
23. Eftink, M. R. (1991) *Methods Biochem. Anal. 35*, 127−205.
24. Cann, A. D., and Kohanski, R. A. (1997) *Biochemistry 36*, 7681−7689.
25. Ho, S. N., Hunt, H. D., Horton, R. M., Pullen, J. K., and Pease, L. R. (1989) *Gene 77*, 51−59.
26. Hasselbacher, C. A., Waxman, E., Galati, L. T., Contino, P. B., Ross, J. B. A., and Laws, W. R. (1991) *J. Phys. Chem. 95*, 2995−3005.
27. Pace, C. N. (1986) *Methods Enzymol. 131*, 266−280.
28. Scholtz, J. M. (1995) *Protein Sci. 4*, 35−43.
29. Santoro, M. M., and Bolen, D. W. (1988) *Biochemistry 27*, 8063−8068.
30. Shortle, D., and Meeker, A. K. (1989) *Biochemistry 28*, 936−944.
31. Chen, Y. H., Yang, J. T., and Chau, K. H. (1974) *Biochemistry 13*, 3350−3359.
32. Woody, R. C. (1995) *Methods Enzymol. 246*, 34−71.
33. Gross, M., Lustig, A., Wallimann, T., and Furter, R. (1995) *Biochemistry 34*, 10350−10357.
34. Bolen, D. W., and Santoro, M. M. (1988) *Biochemistry 27*, 8069−8074.
35. Steer, B. A., and Merrill, A. R. (1995) *Biochemistry 34*, 7225−7233.
36. Cobb, M. H., Sang, B. C., Gonzalez, R., Goldsmith, E., and Ellis, L. (1989) *J. Biol. Chem. 264*, 18701−18706.
37. Wei, L., Hubbard, S. R., Hendrickson, W. A., and Ellis, L. (1995) *J. Biol. Chem. 270*, 8122−8130.
38. Knighton, D. R., Zheng, J., Eyck, L. F. T., Ashford, V. A., Xuong, N.-H., Taylor, S. S., and Sowadski, J. M. (1991) *Science 253*, 407−414.
39. De Bondt, H. L., Rosenblatt, J., Jancarik, J., Jones, H. D., Morgan, D. O., and Kim, S. H. (1993) *Nature 363*, 595−602.
40. Zhang, F., Strand, A., Robbins, D., Cobb, M. H., and Goldsmith, E. J. (1994) *Nature 367*, 704−711.
41. Xu, W., Harrison, S. C., and Eck, M. J. (1997) *Nature 385*, 595−602.
42. Sicheri, F., Moarefi, I., and Kuriyan, J. (1997) *Nature 385*, 602−609.
43. Russo, A. A., Jeffrey, P. D., and Pavletich, N. P. (1996) *Nat. Struct. Biol. 3*, 696−700.
44. Williams, J. C., Wierenga, R. K., and Saraste, M. (1998) *Trends Biochem. Sci. 23*, 179−184.
45. Hanks, S. K., and Quinn, A. M. (1991) *Methods Enzymol. 200*, 38−62.
46. Goldberg, J., Nairn, A. C., and Kuriyan, J. (1996) *Cell 84*, 875−887.
47. Meador, W. E., Means, A. R., and Quiocho, F. A. (1993) *Science 262*, 1718−1721.
48. Nosworthy, N. J., Peterkofsky, A., Konig, S., Seok, Y. J., Szczepanowski, R. H., and Ginsburg, A. (1998) *Biochemistry 37*, 6718−6726.
49. Huffine, M. E., and Scholtz, J. M. (1996) *J. Biol. Chem. 271*, 28898−28902.
50. Pullen, K., Rajagopal, P., Branchini, B. R., Huffine, M. E., Reizer, J., Saier, M. H., Jr., Scholtz, J. M., and Klevit, R. E. (1995) *Protein Sci. 4*, 2478−2486.
51. Meadow, N. D., Fox, D. K., and Roseman, S. (1990) *Annu. Rev. Biochem. 59*, 497−542.
52. Chen, Y., and Barkley, M. D. (1998) *Biochemistry 37*, 9976−9982.
53. Sayle, R. A., and Milner-White, E. J. (1995) *Trends Biochem. Sci. 20*, 374−376.

BI982546S